



## Facile synthesis of goethite anchored regenerated graphene oxide nanocomposite and its application in the removal of fluoride from drinking water

Yunfang Fan<sup>a</sup>, Dandan Fu<sup>a</sup>, Siqi Zhou<sup>a</sup>, Yiqing Lu<sup>a</sup>, Xiaoxi Zhao<sup>a</sup>, Wei Jin<sup>b,\*</sup>,  
Yaping Zhao<sup>a,\*</sup>

<sup>a</sup>Shanghai Key Laboratory for Urban Ecological Process and Eco-Restoration, School of Ecology and Environmental Science, East China Normal University, Shanghai 200241, China, emails: ffyunfang@163.com (Y. Fan), 18656998181@163.com (D. Fu), zhousiqijx@163.com (S. Zhou), luyq1618@163.com (Y. Lu), zxx1881827@126.com (X. Zhao), Tel. +86 21 54341241; email: ypzhaod@des.ecnu.edu.cn (Y.P. Zhao)

<sup>b</sup>School of Environmental Science and Engineering, Tongji University, Shanghai 200092, China, email: tjjinwei@tongji.edu.cn

Received 3 December 2015; Accepted 12 April 2016

### ABSTRACT

Drinking water fluoride pollution is a worldwide environmental problem imposing serious menace to human health. Goethite anchoring regenerated graphene oxide ( $\alpha$ -FeOOH@rGO) nanocomposite was synthesized via facile one-step hydrolysis pathway with ferrous sulfate as starting material. Fluoride adsorption efficiencies in aqueous solution were also testified through batch adsorption experiments.  $\alpha$ -FeOOH@rGO has good defluoridation ability in a wide range of pH and has a strong anti-interference ability in the presence of high concentration foreign anions. Pseudo-second-order adsorption kinetics and Langmuir adsorption isotherms are fitted well involved in fluoride adsorption process. The FTIR and XPS results prove that defluoridation proceeds through an ion-exchange mechanism with sulfate-bearing in  $\alpha$ -FeOOH@rGO crystal structure. It would be useful for the purpose of environmental protection in design and improvement of  $\alpha$ -FeOOH@rGO as a cost-effective anion-exchange adsorbent.

*Keywords:* Fluoride; Adsorption; Iron (oxy)hydroxide; Graphene; Ion exchange

### 1. Introduction

Fluoride is generally released into subsoil water from minerals, geochemical deposits, and anthropogenic sources [1]. Excessive fluoride in drinking water has become a serious environmental problem affecting millions of people in various regions in the world, such as India, Sri Lanka, the Middle East,

Africa, and China [2–4]. The World Health Organization (WHO) recommends that the concentration of fluoride in drinking water should be less than 1.5 mg L<sup>-1</sup> [5]. This concern greatly promotes the water community for searching an effective way of defluoridation. The traditional methods of defluoridation from drinking water include liming and precipitation, membrane, and adsorption techniques [6]. The adsorption process is widely used and can successfully reduce fluoride to an acceptable level [7]. The most crucial part of

\*Corresponding authors.

adsorption is to choose an ideal adsorbent which should be efficient, low-cost, easily regenerated, and environmental-friendly.

The effectiveness of an adsorbent greatly depends on the physicochemical properties of the adsorbent materials. Micro or nano-scale iron-containing adsorbents have demonstrated high adsorption kinetics and high adsorption capacity towards fluoride due to its large surface area. Thanks to natural abundance, unique adsorption, high reactivity, ion exchange capacity, and iron (oxy)hydroxide has been widely applied. However, iron (oxy)hydroxide nanoparticles are easy to agglomerate to decrease the adsorption activity and difficult to be separated from water phase for its nano size effect. Loading iron (oxy)hydroxide on certain carriers would be another alternative to facilitate iron (oxy)hydroxide to application and reclamation [6,8]. Therefore, the novel iron (oxy)hydroxide carriers of high specific surface area and chemical stability are in demand for defluoridation.

Graphene oxide (GO), a derivative of graphene, has a better hydrophilicity and dispersity in solution for its epoxy and hydroxyl groups within the graphene sheets and carboxyl and carbonyl groups at the sheet edges [9–11]. Its oxygen-containing groups can strengthen the interactions between the GO sheets and other laden material, making the combination much easier. Its huge specific surface area and layered structure make it an excellent and applicable carrier comparing other carriers such as carbon nanotube, zeolite, or functionalized polymeric materials, which can provide nanoparticles more accessible reactive centers. Currently, the composites of GO and iron oxide are mostly reported for their application in fuel cells and supercapacitors [12]. The study of defluoridation is rarely reported and it will play an important role in environmental application.

Combining the favorable properties of iron (oxy)hydroxide with GO, this study prepared a novel adsorbent  $\alpha$ -FeOOH@rGO with a convenient method. Dispersing  $\alpha$ -FeOOH uniformly on the rGO sheets can inhibit the aggregation of GO and  $\alpha$ -FeOOH nanoparticles from each other. The primary objectives were to testify the feasibility and efficiency of  $\alpha$ -FeOOH@rGO nanocomposites, by characterizing and analyzing its fluoride removal efficiency, usable pH range, the effect of co-existing anions, and regeneration ability. The exploring adsorption mechanism may contribute to improve fluoride removal efficiency by designing novel structural anions-bearing adsorbent. It will be very useful to know about the environmental interface reaction of fluoride adsorption by iron-containing minerals.

## 2. Materials and methods

### 2.1. Chemical reagents

Sodium fluoride (NaF) is prepared into 1,000 mg L<sup>-1</sup> stock solution stored in polyethylene bottle at 0°C. Graphite powder was purchased from Guangfu fine chemical research institute (Tianjin, China). Sodium fluoride (NaF), ferrous sulfate heptahydrate (FeSO<sub>4</sub>·7H<sub>2</sub>O), potassium nitrate (KNO<sub>3</sub>), potassium permanganate (KMnO<sub>4</sub>), ethylene glycol (EG), hydrogen peroxide (H<sub>2</sub>O<sub>2</sub>, 30%), hydrochloric acid (HCl), and concentrated sulfuric acid (H<sub>2</sub>SO<sub>4</sub>, 98%) were purchased from Sinopharm chemical reagent company (Shanghai, China). All the chemicals were of reagent grade and used without further treatment. Deionized water (DI) is used throughout the experiment.

### 2.2. Preparation and characterization of $\alpha$ -FeOOH@rGO

GO was synthesized using natural graphite powder as the original material by a modified Hummer's method [13].  $\alpha$ -FeOOH@rGO was synthesized briefly as: 0.1 g GO was dissolved in 80 mL water, then 5.56 g FeSO<sub>4</sub>·7H<sub>2</sub>O and 20 mL EG were added into it. The above solution was heated at 80°C for 4 h with agitation. The resulting black precipitates were collected by centrifugation and washed with DI repeatedly and dried at 60°C. The material was then manually powdered and stored in an airtight container for further use. Goethite ( $\alpha$ -FeOOH) was synthesized in a typical way of  $\alpha$ -FeOOH@rGO without GO.

The phase compositions of the as-prepared products were characterized with X-ray diffraction (XRD, Ultima IV, Rigaku, Japan), in the range of 5°–70° with a Cu K $\alpha$  radiation, at wavelength of 1.54056 Å. Fourier transform infrared spectroscopy (FTIR) spectra were recorded using Nicolet FTIR instrument in the 400–4000 cm<sup>-1</sup> region. Scanning electron microscopy images of the product were taken on a field emission scanning electron microscope (SEM, S-4800, Hitachi, Japan). Transmission electron microscopy (TEM, HT7700, Hitachi, Japan) measurements were carried out using a real time charge coupled device camera. X-ray photoelectron spectroscopy (XPS) spectra were acquired with a Kratos Axis Ultra<sup>DLD</sup> spectrometer (Kratos Analytical-A Shimadzu group company, Japan) using a monochromatic Al K $\alpha$  source (1,486.6 eV).

### 2.3. Batch adsorption experiments

The adsorption experiments were carried out in 100 mL glass conical flasks containing 25 mg of the

adsorbent, followed by adding 20 mL of 25 mg L<sup>-1</sup> fluoride solution. The initial pH values of the solutions were adjusted using either 0.1 M HCl or 0.1 M NaOH with a pH meter (PHS-3C, INESA, Shanghai, China). The adsorption isotherm was obtained by changing the initial fluoride concentration from 10 to 200 mg L<sup>-1</sup>. Then, the flasks were shaken at a water bath shaker (HZS-H, Dongming medical instrument factory in Harbin, China) at the rate of 160 rpm for 24 h at 25°C. After completing the experiment, each sample was filtered through a 0.45 μm membrane, and the residual fluoride ion concentration was determined using a spectrophotometer (7200, UNIC, Shanghai, China). Analysis method is according to the national environmental protection standards of the People's Republic of China (HJ 488-2009). The iron leaking was detected by ICP-OES with detection limit of 0.03 mg/L (OPTIMA8000, PE, USA).

Initially, 300 ml fluoride concentrations of 10, 25, and 50 mg L<sup>-1</sup> were added with 500 mg of adsorbent to study the adsorption kinetics at different temperature, respectively. The effect of common ions such as sulfate, chloride, nitrate, bicarbonate, silicate, phosphate, and humic acid (HA) upon the adsorption process was studied by adding required amount of anions (250 mg L<sup>-1</sup> of SO<sub>4</sub><sup>2-</sup>, Cl<sup>-</sup>, NO<sub>3</sub><sup>-</sup>, and HCO<sub>3</sub><sup>-</sup>, respectively, 25 mg L<sup>-1</sup> of SiO<sub>3</sub><sup>2-</sup> and PO<sub>4</sub><sup>3-</sup>, and 20 mg L<sup>-1</sup> of HA) to 20 mL of 25 mg L<sup>-1</sup> fluoride solutions. The reusability of adsorbent was tested by generating via 1 M NaOH or 1 M HCl treatment. Other procedures were the same with that of aforementioned.

### 3. Results and discussion

#### 3.1. Characterization of α-FeOOH@rGO

Goethite is one of the polymorphs of iron oxyhydroxide (FeOOH) and its environmental functions are related to crystalline structure. Fig. 1 shows the XRD patterns of GO, rGO, α-FeOOH, and α-FeOOH@rGO. The broad  $d_{002}$  peak of the rGO at  $2\theta = 26.5^\circ$  indicated an interlayer spacing of 0.336 nm according to Bragg's Equation. The sharp and narrow peak at  $2\theta = 10.6^\circ$  can be assigned to crystal characteristic diffraction peak  $d_{001}$  of GO with the interlayer spacing of 0.834 nm which is larger than that of rGO. The increased interplanar spacing results from the presence of abundant oxygen containing functional groups causing a highly hydrophilic propriety. The peak at  $2\theta = 21.2^\circ, 33.2^\circ, 35.5^\circ, 36.1^\circ, 39.1^\circ, 41.2^\circ, 53.2^\circ, 57.4^\circ,$  and  $61.4^\circ$  can be indexed to (1 1 0), (1 3 0), (1 0 1), (0 4 0), (2 0 0), (1 4 0), (2 2 1), (2 3 1), and (0 0 2) of the

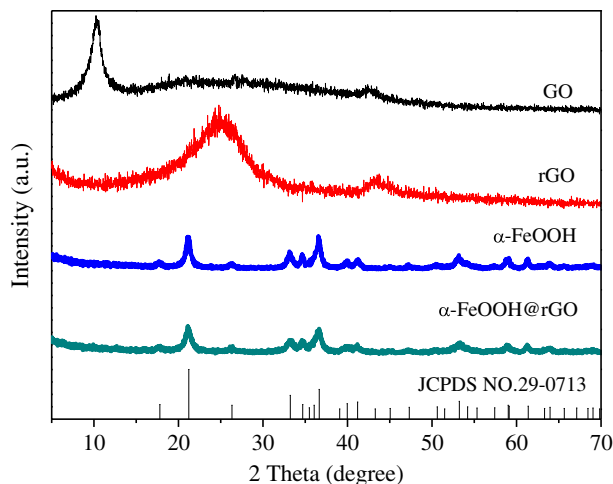


Fig. 1. XRD patterns of GO, rGO, α-FeOOH, and α-FeOOH@rGO.

planes of α-FeOOH and α-FeOOH@rGO, fitting well with the JCPDS card (No.29-0713). The diffraction peak of rGO at  $26.5^\circ$  of α-FeOOH@rGO totally disappeared, suggesting that the layered rGO reduced by Fe<sup>2+</sup> has been fully covered and exfoliated by the formed α-FeOOH nanoparticles. No other apparent diffraction peaks have been found in the pattern of α-FeOOH@rGO suggesting the high purity of α-FeOOH. Based on the (1 1 0) diffraction peaks, the average particle size of α-FeOOH is 9.96 nm estimated by Scherer's Equation. The surface texture and morphology of α-FeOOH@rGO were observed using SEM and TEM as shown in Fig. 2. The SEM image of Fig. 2(A) exhibits a wrinkled sheet structure of rGO. The SEM images of α-FeOOH (Fig. 2(B)) show rod-like morphological structure with high aggregation. According to the SEM images of the α-FeOOH@rGO (Fig. 2(C) and (D)), the nanosize raft-like α-FeOOH particles were evident and well dispersed on the surface of rGO. TEM images (Fig. 2(E)–(H)) show morphology of nanophase rafts consisting of smaller nanorods. The difference of morphology illustrates that α-FeOOH and rGO are combined closely and α-FeOOH dispersed uniformly on the surface of the rGO sheet.

In this study, ferrous sulfate was chosen to produce goethite precipitate and reduce GO simultaneously. Fe<sup>2+</sup> source may adsorb onto the GO sheets due to the coordination of carboxyl, epoxy, and hydroxyl groups through electrostatic interactions to form C–O–Fe bonds, and then generate crystal nuclei sites to form primary particles of α-FeOOH. It is now generally believed that rafts-like particles (shown in HRTEM Fig. 2(G) and (H)) precipitate directly in

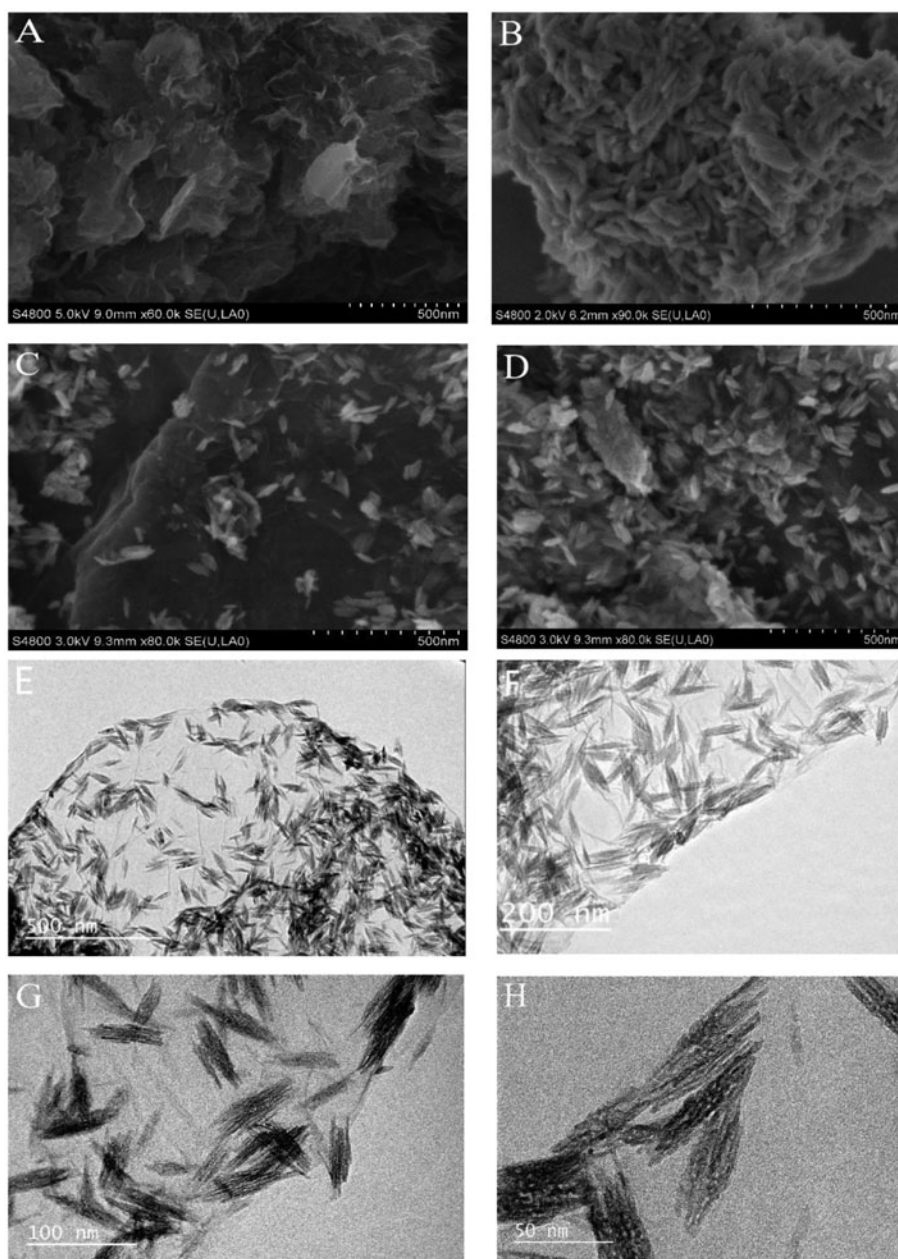


Fig. 2. SEM images of rGO (A),  $\alpha$ -FeOOH (B),  $\alpha$ -FeOOH@rGO (C and D), and TEM images of  $\alpha$ -FeOOH@rGO in different magnifications (E, F, G, and H).

solution via the lateral oriented side-by-side-attached crystal growth pathway in sulfate system with faster growth kinetics [14]. GO does change the nucleation and growth of the  $\alpha$ -FeOOH compared with morphology of  $\alpha$ -FeOOH in the homogeneous precipitation process. These results reveal that GO helps to hinder the aggregation of  $\alpha$ -FeOOH, and vice versa. The high dispersion of  $\alpha$ -FeOOH on rGO will provide large amount of accessible chelating iron center.

### 3.2. Effect of pH

The effect of solution pH on adsorption of fluoride from the aqueous medium is shown in Fig. 3. The adsorption rates of fluoride were between 83.7 and 87.4% during pH range from 2.90 to 10.90, then adsorption rate slightly decrease to 77.1% when pH continuously increases to 12.13. As we all know that the  $pH_{zpc}$  (zero point of charge) of  $\alpha$ -FeOOH is about

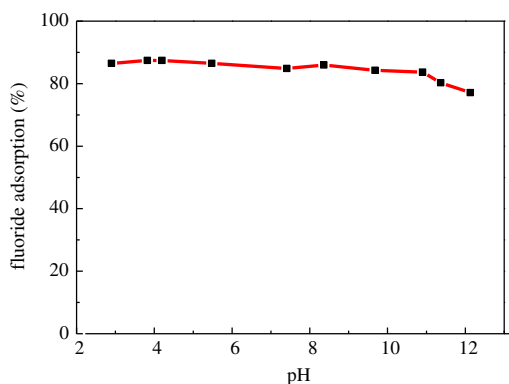


Fig. 3. Effect of solution pH on fluoride adsorption.

9.5 [14]. From neutral to acid pH, i.e. solution  $\text{pH} < \text{pH}_{\text{zpc}}$ ,  $\alpha\text{-FeOOH}$  produces a positively charged surface which show best affinity towards fluoride due to electrostatic attraction. At  $\text{pH} > 9.5$ , the negatively charged surface of  $\alpha\text{-FeOOH}$  resulting in repelling the fluoride ions causing the decline of adsorption capacity. With the alkali increase, the electrostatic repulsion of fluoride ions with the negatively charged surface of  $\alpha\text{-FeOOH}$  increased, especially at  $\text{pH} > 10.9$ . There is a competition between excessive amount of hydroxyl ions and fluoride ions on the active adsorption sites. It causes slow release of adsorbed fluoride ions from the adsorbent's surface. It was reported that the desorption of fluoride at high pH is due to the increased repulsive forces between the negatively charged adsorbent surface and negatively charged fluoride ions in solution as well as the competition between increased concentration of  $\text{OH}^-$  at high pH.

At natural environmental pH conditions (6.5–8.5), fluoride ions must be stably bonded to surface of  $\alpha\text{-FeOOH@rGO}$ . Negligible release of iron is below the detection limit of  $0.03 \text{ mg L}^{-1}$  within the studied pH range. The pH doesn't greatly influence the fluoride adsorption rate, which shows that the adsorption mechanism is chemical ion-exchange in nature. The usable pH range of  $\alpha\text{-FeOOH@rGO}$  is much wider than the previous studies of fluoride adsorption [15–17]. The maximum adsorption capacity of  $\text{BAS@GHG-2}$  reaches at pH 7.2. Further increases or decreases the pH, it causes adsorption capacity to decrease about 40% [16]. Similar studies of maxima in acidic pH range have been widely reported [16]. Oppositely, desorption effect is good in alkaline pH range. Just as Zr loaded collagen fiber, more than 97.0% of the fluoride could be desorbed at pH 11.5 [18]. It happens that there is a similar case, as the pH increases above six, the fluoride starts to dissolve into the solution from rare earth oxides, with more than

95% of the fluoride desorbed at pH 12. Thus, one of the advantages of the  $\alpha\text{-FeOOH@rGO}$  adsorbent materials is that it allows a wide usable pH range throughout the adsorption process.

### 3.3. Adsorption kinetics

In order to obtain the adsorption efficiency, the effect of contact time on defluoridation by  $\alpha\text{-FeOOH@rGO}$  is shown in Fig. 4. It illustrates that 80% adsorption of the fluoride occurred in the initial 20 min and then reached the equilibrium within 1 h. Equilibrium adsorption capacity decreased with the temperature and increased with the initial fluoride concentrations. The pseudo-first-order rate equation and pseudo-second-order rate equations were evaluated based on the experimental data [19,20]:

$$\log(q_e - q_t) = \log\left(q_e - \frac{k_1}{2.303} t\right) \quad (1)$$

$$\frac{t}{q_t} = \frac{1}{k_2 q_e^2} + \frac{1}{q_e} t \quad (2)$$

where  $q_e$  and  $q_t$  are the amount of fluoride adsorbed on adsorbent (mg/g) at equilibrium and at any time  $t$  (minute), respectively.  $k_1$  and  $k_2$  stand for the pseudo-first-order rate and pseudo-second-order rate constants of adsorption. The results of fitting models are showed in Fig. 4, and the parameter values obtained by curve-fitting kinetic data are listed in Table 1. Based on the correlation coefficient, pseudo-second-order rate equation is more suitable to describe adsorption kinetics of fluoride whether at different temperature or different initial fluoride concentrations. It shows that a distinct fast diffusion pathway controlling the initial adsorption kinetics followed by relatively slow diffusion prior to adsorption equilibrium. This indicates that  $\alpha\text{-FeOOH@rGO}$  initially provides larger accessible surface areas and stronger reaction activity for fluoride and then slow diffusion of fluoride due to the aggregation inside the tunnel structure of  $\alpha\text{-FeOOH}$ . It suggests that  $\alpha\text{-FeOOH@rGO}$  may have a heterogeneity surface, and that a chemisorption step may be dominant in the rate of adsorption process.

### 3.4. Adsorption isotherms

The Langmuir and Freundlich isotherm equations are most widely used to describe the adsorption capacity of a sorbent. Langmuir isotherm model is

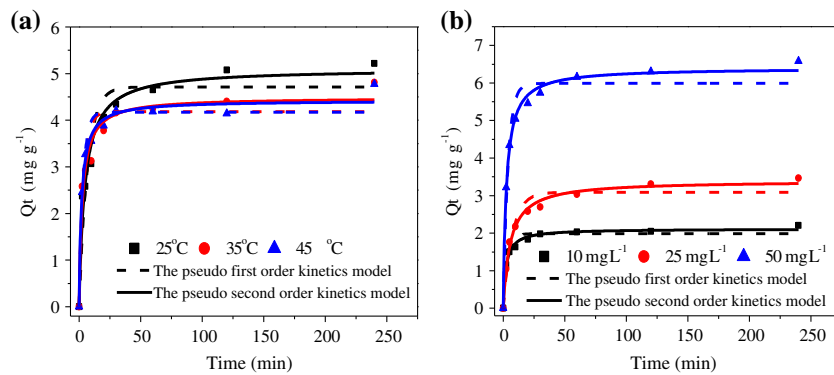


Fig. 4. The effect of temperature (a) and fluoride concentration (b) on fluoride adsorption kinetics by  $\alpha$ -FeOOH@rGO.

Table 1  
Kinetic parameters for fluoride adsorption by  $\alpha$ -FeOOH@rGO

	Pseudo-first-order			Pseudo-second-order		
	$q_e$ (mg g <sup>-1</sup> )	$k_1$ (min <sup>-1</sup> )	$R^2$	$q_e$ (mg g <sup>-1</sup> )	$k_2$ (min <sup>-1</sup> )	$R^2$
25 °C	4.7135	0.1483	0.9058	5.1043	0.0426	0.9684
35 °C	4.1861	0.2591	0.8987	4.4872	0.0860	0.9653
45 °C	4.1720	0.3115	0.9532	4.4251	0.1112	0.9823
10 mg L <sup>-1</sup>	1.9870	0.2905	0.9526	2.1147	0.2123	0.9906
25 mg L <sup>-1</sup>	3.0897	0.1360	0.9443	3.3976	0.0529	0.9900
50 mg L <sup>-1</sup>	5.9899	0.2601	0.9613	6.4025	0.0609	0.9950

applied to describe the monolayer adsorption, which assumes the surface with homogeneous binding sites, equivalent adsorption energies, and no interaction among adsorbed molecules. Freundlich isotherm model is an empirical model, which is applied to multilayer adsorption of heterogeneous surfaces, with the interaction between adsorbed species. The mathematical expressions of these two models are as follows:

Langmuir isotherm model:

$$q_e = \frac{q_{\max} b C_e}{1 + b C_e} \quad (3)$$

Freundlich isotherm model:

$$q_e = K_F C_e^{\frac{1}{n}} \quad (4)$$

where  $C_e$  (mg L<sup>-1</sup>) and  $q_e$  (mg g<sup>-1</sup>) are the concentration and adsorption capacity at equilibrium, respectively;  $q_{\max}$  (mg g<sup>-1</sup>) is the maximum amount of adsorption;  $b$  (L mg<sup>-1</sup>) is an affinity constant related to the energy of adsorption;  $K_F$  (mg<sup>1-1/n</sup> L<sup>1/n</sup>/g) and  $\frac{1}{n}$  represent adsorption capacity and adsorption intensity, respectively.

The fitting results of these two models are shown in Fig. 5 and Table 2. According to the correlation coefficient, Langmuir isotherm model can be used to describe the adsorption of fluoride better than Freundlich isotherm model, suggesting the monolayer adsorption. The maximum adsorption capacity  $q_{\max}$  of  $\alpha$ -FeOOH@rGO was of 24.67 mg g<sup>-1</sup> at 25 °C and the adsorption decreased with the increasing temperature.  $\alpha$ -FeOOH@rGO has a high fluoride affinity compared with that of other sorbents as shown in Table 3.

Thermodynamic parameters were calculated to assess the thermodynamic spontaneity and feasibility of the adsorption process, such as changes in Gibbs free energy ( $\Delta G^\circ$ ), enthalpy ( $\Delta H^\circ$ ), and entropy ( $\Delta S^\circ$ ) (Table 2). Equations are as follows:

$$\Delta G^\circ = -RT \ln(K_0) \quad (5)$$

$$\Delta G^\circ = \Delta H^\circ - T\Delta S^\circ \quad (6)$$

where  $T$  (K) is the temperature,  $R$  (8.314 × 10<sup>-3</sup> kJ mol<sup>-1</sup> K) is the universal gas constant, and  $K_0$  is the thermodynamic equilibrium constant. The thermodynamic equilibrium constant ( $K_0$ ) is determined by plotting  $\ln(q_e/c_e)$  vs.  $q_e$ , and extrapolating to zero  $q_e$  using a graphical method to give the value of  $K_0$ .

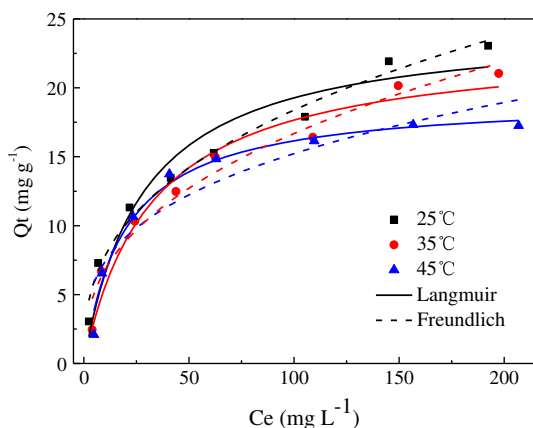


Fig. 5. Adsorption isotherms of fluoride by  $\alpha$ -FeOOH@rGO.

Values of  $\Delta S^\circ$  and  $\Delta H^\circ$  are evaluated from the slope and intersect of plotting  $\Delta G^\circ$  vs.  $T$ . The calculated  $\Delta G^\circ$  value indicated that the fluoride adsorption by  $\alpha$ -FeOOH@rGO is spontaneous and was found to be decreased with increase in temperature. The positive value of  $\Delta H^\circ$  indicates the endothermic nature of the sorption. The negative values of  $\Delta S^\circ$  showed the decreasing randomness during the sorption process [21,22].

### 3.5. Effect of common ions and cycles of reuse

The anti-interference and reusability would be the desired property of a good adsorbent for application. The fluoride-containing drinking water contains many kinds of co-existing ions which may compete with fluoride ions for the active sites during adsorption process. The interaction of common ions on defluoridation by  $\alpha$ -FeOOH@rGO is shown in Fig. 6. The adsorption experiments were based on the concentrations stipulated in Standards for drinking water quality (GB5749–2006). In general, their effect on defluoridation was in the sequence of  $\text{HCO}_3^- > \text{PO}_4^{3-} > \text{SiO}_3^{2-} > \text{SO}_4^{2-} > \text{NO}_3^- > \text{Cl}^-$ . The existence of high concentrations of  $\text{SiO}_3^{2-}$ ,  $\text{PO}_4^{3-}$ ,  $\text{HCO}_3^-$  and HA may cause less than 10% reduction to the adsorption capacity of fluoride. Decreasing the concentration of HA and  $\text{HCO}_3^-$  may alleviate this negative effective.  $\text{SO}_4^{2-}$ ,  $\text{Cl}^-$ , and  $\text{NO}_3^-$  nearly don't influence the fluoride adsorption capacity on the adsorbent. Chen et al. reported that  $\text{PO}_4^{3-}$  and  $\text{CO}_3^{2-}$  nearly exerted about 35% reduction of fluoride adsorption capacity by basic aluminum sulfate (BAS)@GHG-2 while  $\text{SO}_4^{2-}$ ,  $\text{Cl}^-$ , and  $\text{NO}_3^-$  had little effects on fluoride adsorption [15]. Zr-oxalic acid impregnated AC showed a decrease of 44, 49, and 55% on fluoride adsorption capacity when  $\text{SO}_4^{2-}$ ,  $\text{Cl}^-$ ,  $\text{NO}_3^-$ ,  $\text{PO}_4^{3-}$ , and  $\text{CO}_3^{2-}$  were presented in a

Table 2  
Dynamic parameters of the fluoride adsorption by  $\alpha$ -FeOOH@rGO

Temperature (°C)	Langmuir		$R^2$	Freundlich			Thermodynamic parameters		
	$b$ (L mg <sup>-1</sup> )	$q_{\text{max}}$ (mg g <sup>-1</sup> )		$k$	$n$	$R^2$	$\Delta G^\circ$ (kJ mol <sup>-1</sup> )	$\Delta H^\circ$ (kJ mol <sup>-1</sup> )	$\Delta S^\circ$ (kJ mol <sup>-1</sup> K)
25	0.0162	24.6722	0.9949	1.6456	2.1249	0.9612	-4.412	37.13	-0.109
35	0.0186	22.4716	0.9924	1.7643	2.2420	0.9516	-3.717		
45	0.0188	19.4472	0.9805	1.5689	2.2673	0.9294	-2.225		

Table 3  
Comparison of fluoride adsorption capacity and equilibration time with different adsorbents

Adsorbents	Fluoride adsorption capacity (mg g <sup>-1</sup> )	Adsorption equilibration time (h)	Refs.
Fe(III)-carboxylated chitosan	4.23	0.67	[22]
Granular ferric hydroxide	7.00	1	[23]
Hydrous ferric oxide doped alginate beads	8.90	4	[24]
Graphene	17.65	1	[25]
PPy/Fe <sub>3</sub> O <sub>4</sub> nanocomposite	17.60–22.30	24	[26]
Fe <sub>3</sub> O <sub>4</sub> @Al(OH) <sub>3</sub>	88.48	4	[27]
$\alpha$ -FeOOH@rGO	24.67	1	This study

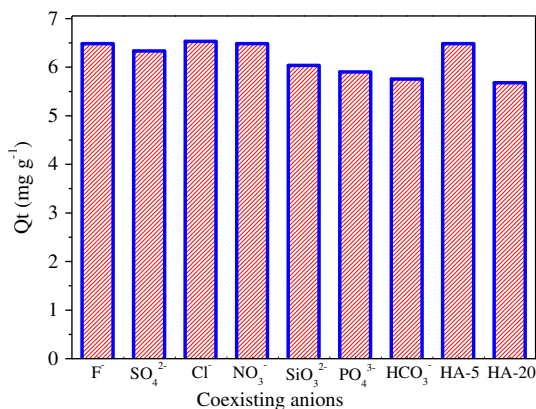


Fig. 6. Effect of common ions on fluoride adsorption by  $\alpha$ -FeOOH@rGO.

mixture of 1, 10, or 50 mg L<sup>-1</sup>, respectively [28]. From the results, adsorption center  $\alpha$ -FeOOH has a better anti-interference ability or high selectivity, especially for the disposal of the drinking water with a high concentration of SiO<sub>3</sub><sup>2-</sup>, PO<sub>4</sub><sup>3-</sup>, HCO<sub>3</sub><sup>-</sup>, and HA.

Furthermore, to evaluate the regeneration and recyclability of  $\alpha$ -FeOOH@rGO nanocomposites, six consecutive adsorption–desorption cycles were performed by repeated washing with HCl and NaOH solutions. The percentage of adsorption of fluoride by  $\alpha$ -FeOOH@rGO was discovered to be reduced from 54 to 12% following a sequence of regeneration (shown in Fig. 7). After first adsorption, a lot of the surface adsorption sites were occupied by the fluoride. With the adsorption continuing, available sites on the goethite surface subsequently decreased, so the adsorption capacity of  $\alpha$ -FeOOH@rGO would be decreased accordingly. The results suggest that the prepared  $\alpha$ -FeOOH@rGO adsorbent could be partly regenerated via NaOH and HCl treatment. The regenerated mechanism would be the ion-exchange through Cl<sup>-</sup>/OH<sup>-</sup> with F<sup>-</sup> adsorbed on the surface of sorbent [30,31]. The iron leaching should be considered when using HCl regenerant. Based on this research, better regenerated methods should be developed for  $\alpha$ -FeOOH@rGO practical use in a continuous cycle of operation.

### 3.6. Adsorption mechanism of fluoride

The defluoridation mechanism by  $\alpha$ -FeOOH@rGO was revealed by FTIR and XPS. The FTIR spectra of  $\alpha$ -FeOOH@rGO before and after fluoride adsorption are shown in Fig. 8. The FTIR spectrum of  $\alpha$ -FeOOH@rGO shows certain IR bands chiefly related to the characteristics of  $\alpha$ -FeOOH [32]. The IR band at 3,417 cm<sup>-1</sup> is due to the presence of the surface H<sub>2</sub>O molecules,

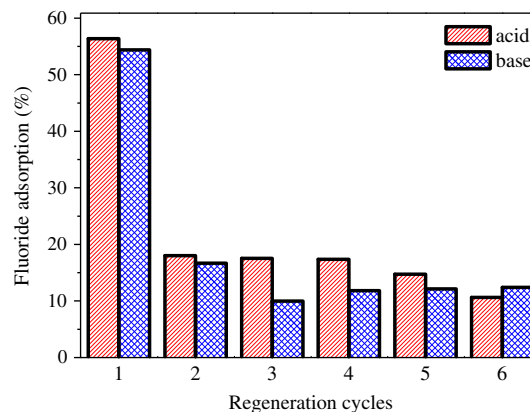


Fig. 7. Recycling ability of  $\alpha$ -FeOOH@rGO in different fluoride adsorption cycles.

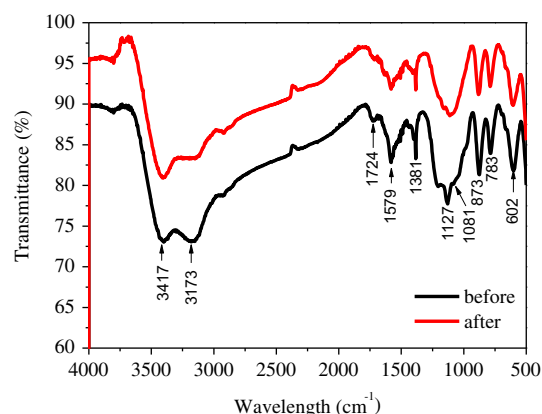


Fig. 8. FTIR pattern of  $\alpha$ -FeOOH@rGO before and after adsorption of fluoride.

whereas the band at 3,173 cm<sup>-1</sup> is attributed to the hydrogen bonded surface OH group stretching mode in  $\alpha$ -FeOOH [33]. The band at 2,909 and 1,724 cm<sup>-1</sup> are stretching vibrations of C–H in organic chain and ester carbonyl group, respectively. Two bands at 1,127 and 1,081 cm<sup>-1</sup> are attributed to the splitted strong  $\nu_3$  SO<sub>4</sub> mode. The low splitting bands observed may indicate that the symmetric of bearing sulfate is lowered due to a non-symmetric interaction which exists between Fe<sup>3+</sup> cations and chelating water molecules in the FeO<sub>3</sub>(OH)<sub>3</sub> octahedral structure with one of the oxygen atom of the sulfate anion. In the low frequency region, the IR band at 873 and 783 cm<sup>-1</sup> can be typically assigned to Fe–O–H bending vibrations in  $\alpha$ -FeOOH. The IR band at 604 cm<sup>-1</sup> can be ascribed to Fe–O stretching vibration, and is influenced by the shape of the  $\alpha$ -FeOOH. The FTIR spectra of fluoride absorbed  $\alpha$ -FeOOH@rGO show that the intensity of absorption band at 3,173 cm<sup>-1</sup> assigned to the

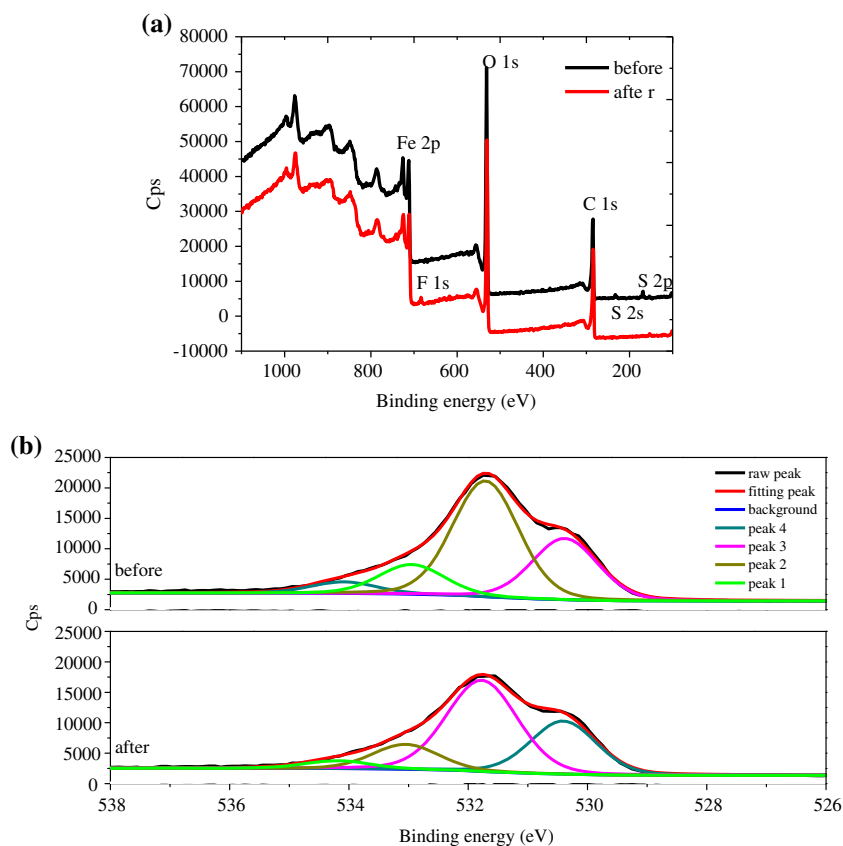


Fig. 9. Wide scan XPS spectra of  $\alpha$ -FeOOH@GO before and after fluoride adsorption (a) and XPS spectra of O 1s deconvolution (b).

Table 4

Binding energy of Fe 2p, O 1s, and C 1s and atomic surface concentrations of the detected elements for  $\alpha$ -FeOOH@GO before and after fluoride adsorption

Binding energy (eV)									
	Fe 2p		O 1s			F 1s	S 2s	C 1s	
Before	711.2	726.5	530.4	531.7	533.0	534.1	No	232.4	284.7
After	711.2	726.6	530.4	531.7	533.0	534.1	684.4	No	284.8
Atomic surface concentration (%)									
	Fe	O				F	S	C	
		Fe-O <sub>oxides</sub>	Fe-OH	Fe-OH <sub>ads</sub>	H <sub>2</sub> O <sub>ads</sub>				
Before	6.52	39.14				0	0.93	53.41	
		28.1%	53.1%	13.5%	5.3%				
After	7.86	35.02				0.89	0	56.24	
		29.1%	53.4%	13.0%	4.5%				

physically adsorbed water from air reduces, which may indicate the involvement of this functional group in the uptake of fluoride [34]. Peak observed for sulfate near  $1,127\text{ cm}^{-1}$  vanishes in case of fluoride absorbed  $\alpha$ -FeOOH@rGO, indicating the participation

in this anion-exchange process. This indicated that fluoride was bound through Fe–O bonding to form surface complex.

In Fig. 9, XPS shows the chemical environment of the  $\alpha$ -FeOOH@rGO before and after the adsorption of

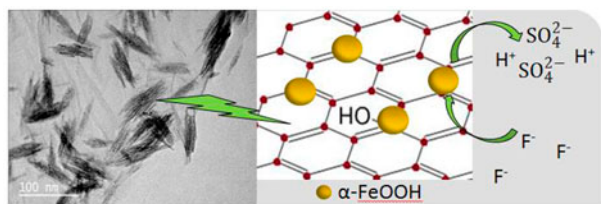


Fig. 10. Proposed fluoride adsorption mechanism by  $\alpha$ -FeOOH@rGO.

fluoride. In the XPS wide scan spectrum, the peaks located at 711.2, 531.7, and 284.7 eV are assigned to the characteristic peaks of Fe 2p, O 1s, and C 1s, respectively, which show the existence of GO and  $\alpha$ -FeOOH. Meanwhile, Fe 2p was deconvoluted into two major peaks with binding energies at 711.2–726.6 eV, corresponding to Fe 2p<sub>3/2</sub> and Fe 2p<sub>1/2</sub>, respectively, the energy separation is 15.4 eV, which is characteristic of Fe<sup>3+</sup> in FeOOH. In the sample before fluoride adsorption S 2s and S 2p peak are observed around 232.4 and 168.7 eV are also detected, indicating that sulfate anions incorporated into the goethite, thus the  $\alpha$ -FeOOH crystal structure is iron (oxy)hydroxide containing sulfate [35]. Comparing with the sample after fluoride adsorption, S 2s and S 2p peaks disappear and the F 1s peak located at 684.4 eV appears. This phenomenon indicates SO<sub>4</sub><sup>2-</sup> take part in the anion exchange with F<sup>-</sup> in the process of adsorption. Compared with hydroxide ions, sulfates have lower affinity for iron, therefore, in the thermodynamic sense, it is easier to replace sulfate with fluoride than hydroxide ions. In Fig. 9(b), the O 1s region could be deconvoluted into four overlapped peaks at 530.4, 531.7, 534, and 534.1 eV, corresponding to Fe–O<sub>oxide</sub> and Fe–OH in lattice structure oxygen, Fe–OH<sub>ads</sub> and H<sub>2</sub>O<sub>ads</sub> in adsorbed oxygen. However, in Table 4, only the content of H<sub>2</sub>O is changed (5.3% before adsorption and 4.5% after adsorption of fluoride) suggesting the releasing of free H<sup>+</sup> to the solution from adsorbed H<sub>2</sub>O of  $\alpha$ -FeOOH@rGO which was also proved by the decreasing in solution pH after fluoride adsorption. The substitution reaction of OH<sup>-</sup> in the structure of  $\alpha$ -FeOOH was not obvious [36]. Thus, the proposed fluoride adsorption mechanisms (shown in Fig. 10) were based on the ion-exchange with the  $\alpha$ -FeOOH@rGO containing sulfate anions accompanying the releasing of H<sup>+</sup> into the solution, which is in accordance with the result of FTIR in Fig. 8. Consequently, the adsorption capacity of goethite is improved due to the existence of sulfate. Usually, anions adsorption on metal oxide surface is through coulombic forces and/or ligand exchange reactions, where the anions displace OH<sup>-</sup> or H<sub>2</sub>O from the surface [37]. Fluoride is

believed to replace singly coordinated Fe–OH groups from the surface of goethite usually [38]. Velazquez-Jimenez et al. also proposed fluoride adsorption mechanisms were a hydroxyl exchange from the Zr-oxalic acid impregnated AC surface sites [29]. Due to the heterogeneity of the adsorption sites, the adsorption reaction mechanism may be complex. This adsorption mechanism provides us with a new perspective to improve the performance of adsorbent to synthesize metal oxides with high content of the surface exchangeable anions.

#### 4. Conclusions

This study prepared  $\alpha$ -FeOOH@rGO hybrid adsorbent in one-step hydrolysis method and characterized through XRD, SEM, and TEM. The raft-like  $\alpha$ -FeOOH was uniformly dispersed on the rGO sheet, which provides fluoride with large amount of accessing adsorption sites.  $\alpha$ -FeOOH@rGO has good defluorination efficiency in a wide range of pH from 3 to 12, pseudo-second-order adsorption kinetic and Langmuir adsorption isotherm are fitted well for fluoride adsorption process. The maximum adsorption capacity of fluoride was 24.67 mg g<sup>-1</sup>.  $\alpha$ -FeOOH@rGO has a strong anti-interference ability in presence of high concentration foreign anions present in drinking water. The FTIR and XPS results proved that the uptake of fluoride by  $\alpha$ -FeOOH@rGO proceeds by an ion-exchange mechanism. The fluoride will exchange with the sulfate contained in  $\alpha$ -FeOOH crystal structure and accompanying with free H<sup>+</sup> releases to the solution. This work demonstrates the important role of the surface sulfate anions in fluoride adsorption, and brings forward an important approach in design and synthesis of metal oxide adsorbents with high content of the surface exchangeable anions. It should be of importance for both theoretical investigations and practical water treatment.

#### Acknowledgements

This research was financed by National Natural Science Foundation of China (No. 21377039) and the Shanghai international cooperation research projects (No. 14230710900).

#### References

- [1] A.A.M. Daifullah, S.M. Yakout, S.A. Elreefy, Adsorption of fluoride in aqueous solutions using KMnO<sub>4</sub>-modified activated carbon derived from steam pyrolysis of rice straw, *J. Hazard. Mater.* 147 (2007) 633–643.

- [2] H. Liu, Y. Gao, L. Sun, M. Li, B. Li, D. Sun, Assessment of relationship on excess fluoride intake from drinking water and carotid atherosclerosis development in adults in fluoride endemic areas, China, *Int. J. Hyg. Environ. Health* 217 (2014) 413–420.
- [3] Ministry of Environmental Protection of the People's Republic of China, Report on the State of the Environment in China, Beijing, 2008.
- [4] S. Ayoob, A.K. Gupta, Sorptive response profile of an adsorbent in the defluoridation of drinking water, *Chem. Eng. J.* 133 (2007) 273–281.
- [5] WHO, Guidelines for Drinking-Water Quality, third ed., vol. 1, Recommendations, Geneva, 2008.
- [6] M. Mohapatra, S. Anand, B.K. Mishra, D.E. Giles, P. Singh, Review of fluoride removal from drinking water, *J. Environ. Manage.* 91 (2009) 67–77.
- [7] K. Biswas, S.K. Saha, U.C. Ghosh, Adsorption of fluoride from aqueous solution by a synthetic iron(III)-aluminum(III) mixed oxide, *Ind. Eng. Chem. Res.* 46 (2007) 5346–5356.
- [8] F. Peng, T. Luo, L. Qiu, Y. Yuan, An easy method to synthesize graphene oxide-FeOOH composites and their potential application in water purification, *Mater. Res. Bull.* 48 (2013) 2180–2185.
- [9] M. Hirata, T. Gotou, S. Horiuchi, M. Fujiwara, M. Ohba, Thin-film particles of graphite oxide: High-yield synthesis and flexibility of the particles, *Carbon* 42 (2004) 2929–2937.
- [10] G.I. Titelman, V. Gelman, S. Bron, R.L. Khalfin, Y. Cohen, H. Bianco-Peled, Characteristics and microstructure of aqueous colloidal dispersions of graphite oxide, *Carbon* 43 (2005) 641–649.
- [11] B. Li, H. Cao, G. Yin, Y. Lu, J. Yin, Cu<sub>2</sub>O@reduced graphene oxide composite for removal of contaminants from water and supercapacitors, *J. Mater. Chem.* 21 (2011) 10645–10648.
- [12] S. Petnikota, S.K. Marka, A. Banerjee, M.V. Reddy, V.V.S.S. Srikanth, B.V.R. Chowdari, Graphenothermal reduction synthesis of 'exfoliated graphene oxide/iron (II) oxide' composite for anode application in lithium ion batteries, *J. Power Sources* 293 (2015) 253–263.
- [13] W.S. Hummers Jr., R.E. Offeman, Preparation of graphitic oxide, *J. Am. Chem. Soc.* 80(6) (1958) 1339–1339.
- [14] T.A. Vu, M.M. Reagan, D.S. Li, B. Legg, J.J.D. Yoreo, J.F. Banfield, H.Z. Zhang, Kinetics of crystal growth of nanogoethite in aqueous solutions containing nitrate and sulfate anions, *Cryst. Eng. Comm.* 16 (2014) 1466–1471.
- [15] M. Mohapatra, K. Rout, P. Singh, S. Anand, S. Layek, H.C. Verma, B.K. Mishra, Fluoride adsorption studies on mixed-phase nano iron oxides prepared by surfactant mediation-precipitation technique, *J. Hazard. Mater.* 186 (2011) 1751–1757.
- [16] Y.Q. Chen, Q.K. Zhang, L.B. Chen, H. Bai, L. Li, Basic aluminum sulfate@graphene hydrogel composites: Preparation and application for removal of fluoride, *J. Mater. Chem. A* 1 (2013) 13101–13110.
- [17] Y.H. Huang, Y.J. Shih, C.C. Chang, Adsorption of fluoride by waste iron oxide: The effects of solution pH, major coexisting anions, and adsorbent calcination temperature, *J. Hazard. Mater.* 186 (2011) 1355–1359.
- [18] X. Liao, B. Shi, Adsorption of fluoride on zirconium (IV)-impregnated collagen fiber, *Environ. Sci. Technol.* 39 (2005) 4628–4632.
- [19] Y.S. Ho, Second-order kinetic model for the sorption of cadmium onto tree fern: A comparison of linear and non-linear methods, *Water Res.* 40 (2006) 119–125.
- [20] V. Sivasankar, S. Muruges, S. Rajkumar, A. Darchen, Cerium dispersed in carbon (CeDC) and its adsorption behavior: A first example of tailored adsorbent for fluoride removal from drinking water, *Chem. Eng. J.* 214 (2013) 45–54.
- [21] R.H. Masue, T.A. Loeppert, T.A. Kramer, Arsenate arsenite adsorption and desorption behaviour on coprecipitated aluminium: Iron hydroxides, *Environ. Sci. Technol.* 41 (2007) 837–842.
- [22] L. Yan, Y. Xu, H. Yu, X. Xin, Q. Wei, B. Du, Adsorption of phosphate from aqueous solution by hydroxy-aluminum, hydroxy-iron and hydroxy-iron-aluminum pillared bentonites, *J. Hazard. Mater.* 179 (2010) 244–250.
- [23] N. Viswanathan, S. Meenakshi, Selective sorption of fluoride using Fe(III) loaded carboxylated chitosan beads, *J. Fluorine Chem.* 129 (2008) 503–509.
- [24] E. Kumar, Defluoridation from aqueous solutions by granular ferric hydroxide (GFH), *Water Res.* 43 (2009) 490–498.
- [25] M.G. Sujana, A. Mishra, B.C. Acharya, Hydrous ferric oxide doped alginate beads for fluoride removal: Adsorption kinetics and equilibrium studies, *Appl. Surf. Sci.* 270 (2013) 767–776.
- [26] Y. Li, P. Zhang, Q. Du, X. Peng, T. Liu, Z. Wang, Y. Xia, W. Zhang, K. Wang, H. Zhu, D. Wu, Adsorption of fluoride from aqueous solution by graphene, *J. Colloid Interface Sci.* 363 (2011) 348–354.
- [27] M. Bhaumik, Removal of fluoride from aqueous solution by polypyrrole/Fe<sub>3</sub>O<sub>4</sub> magnetic nanocomposite, *J. Hazard. Mater.* 186 (2011) 150–159.
- [28] X. Zhao, J. Wang, F. Wu, T. Wang, Y. Cai, Y. Shi, G. Jiang, Removal of fluoride from aqueous media by Fe<sub>3</sub>O<sub>4</sub>@Al(OH)<sub>3</sub> magnetic nanoparticles, *J. Hazard. Mater.* 173 (2010) 102–109.
- [29] L.H. Velazquez-Jimenez, R.H. Hurt, J. Matos, J.R. Rangel-Mendez, Zirconium-carbon hybrid sorbent for removal of fluoride from water: Oxalic acid mediated Zr(IV) assembly and adsorption mechanism, *Environ. Sci. Technol.* 48 (2014) 1166–1174.
- [30] Y. Zhang, Y. Jia, A facile solution approach for the synthesis of akaganéite (β-FeOOH) nanorods and their ion-exchange mechanism toward As(V) ions, *Appl. Surf. Sci.* 290 (2014) 102–106.
- [31] Y. Fu, J. Wang, Q. Liu, H. Zeng, Water-dispersible magnetic nanoparticle-graphene oxide composites for selenium removal, *Carbon* 77 (2014) 710–721.
- [32] L. Verdonck, S. Hoste, F.F. Roelandt, G.P. Van Der Kelen, Normal coordinate analysis of α-FeOOH—A molecular approach, *J. Mol. Struct.* 79 (1982) 273–279.
- [33] C. Morterra, A. Chiorlino, E. Borello, An IR spectroscopic characterization of α-FeOOH (goethite), *Mater. Chem. Phys.* 10 (1984) 119–138.
- [34] S. Jagtap, M.K.N. Yenkie, N. Labhsetwar, S. Rayalu, Defluoridation of drinking water using chitosan based mesoporous alumina, *Microporous Mesoporous Mater.* 142 (2011) 454–463.

- [35] L. Gordon, M.L. Salutsky, H.H. Willard, *Precipitation From Homogeneous Solution*, Wiley, New York, NY, 1959.
- [36] F. Bonnet, F. Ropital, P. Lecour, D. Espinat, Y. Huiban, L. Gengembre, Y. Berthier, P. Marcus, Study of the oxide/carbide transition on iron surfaces during catalytic coke formation, *Surf. Interface Anal.* 34 (2002) 418–422.
- [37] Y. Wang, E.J. Reardon, Activation and regeneration of a soil sorbent for defluoridation of drinking water, *Appl. Geochem.* 16 (2001) 531–539.
- [38] T. Hiemstra, W.H.V. Riemsdijk, Fluoride adsorption on goethite in relation to different types of surface sites, *J. Colloid Interface Sci.* 225 (2000) 94–104.